

A Simplified Lattice Boltzmann Method without Evolution of Distribution Function

Z. Chen¹, C. Shu^{1,*}, Y. Wang¹, L. M. Yang² and D. Tan¹

¹ Department of Mechanical Engineering, National University of Singapore 10 Kent Ridge Crescent, Singapore 119260

² Department of Aerodynamics, College of Aerospace Engineering, Nanjing University of Aeronautics and Astronautics, Yudao Street, Nanjing, Jiangsu 210016, China

Received 10 June 2016; Accepted (in revised version) 17 July 2016

Abstract. In this paper, a simplified lattice Boltzmann method (SLBM) without evolution of the distribution function is developed for simulating incompressible viscous flows. This method is developed from the application of fractional step technique to the macroscopic Navier-Stokes (N-S) equations recovered from lattice Boltzmann equation by using Chapman-Enskog expansion analysis. In SLBM, the equilibrium distribution function is calculated from the macroscopic variables, while the non-equilibrium distribution function is simply evaluated from the difference of two equilibrium distribution functions. Therefore, SLBM tracks the evolution of the macroscopic variables rather than the distribution function. As a result, lower virtual memories are required and physical boundary conditions could be directly implemented. Through numerical test at high Reynolds number, the method shows very nice performance in numerical stability. An accuracy test for the 2D Taylor-Green flow shows that SLBM has the second-order of accuracy in space. More benchmark tests, including the Couette flow, the Poiseuille flow as well as the 2D lid-driven cavity flow, are conducted to further validate the present method; and the simulation results are in good agreement with available data in literatures.

AMS subject classifications: 76M28, 76P99

Key words: Chapman-Enskog expansion analysis, lattice Boltzmann equation, Navier-Stokes equations, memory cost, stability.

1 Introduction

Lattice Boltzmann Method (LBM) [1,2] is becoming a popular method in the field of Computational Fluid Dynamics (CFD). In the last few decades, LBM was being developed

*Corresponding author.
Email: mpeshuc@nus.edu.sg (C. Shu)

continuously [3–14], and has been widely applied in various kinds of fluid problems, including micro flows, thermal flows, multiphase flows and other problems [15–22].

Different from the conventional CFD methods based on the macroscopic Navier-Stokes (N-S) equations [23–27], LBM is a mesoscopic method rooted from the lattice Boltzmann equation (LBE) [28–31]. In LBM, the time marching is reflected in the evolution of the density distribution function. The macroscopic physical properties, such as the density and the velocity, are obtained from the conservation laws on a particular grid point. The evolution process of the density distribution function is realized by two steps: streaming and collision. Specifically, the streaming process is to distribute the effects from a local point to the surrounding points; and the collision process describes the combination effects on a local point. LBM is welcome by the CFD researchers due to several nice features. The first and also the most important feature is its kinetic nature. The simple streaming and collision processes in LBM are able to capture the complex nonlinear phenomenon in physics, and at the same time, avoid the manipulation of complex nonlinear terms or high order derivatives in macroscopic N-S equations. Secondly, LBM solves a set of algebraic equations; and no differential equations are involved, which makes the computation more straightforward and brief. In addition, being an explicit scheme, LBM facilitates the practical coding and parallelization, which makes it suitable to solve engineering problems. Apart from the above appealing characteristics, LBM also suffers from a number of drawbacks. Firstly, due to lattice uniformity, the standard LBM is only applicable on uniform mesh. To apply LBM on non-uniform mesh or for complex geometry, additional computational efforts are needed. The second drawback is that the standard LBM requires more virtual memories compared with the N-S solvers. It is needed to store the distribution functions along all lattice velocity directions at all grid points. Such storage requirement may be a heavy burden for large-scale problems, especially for 3D problems. Finally, it is also inconvenient for the standard LBM to implement the physical boundary conditions. The boundary conditions for the velocity and/or for the pressure need to be transformed into the conditions for the density distribution functions. Therefore, for problems with complex boundaries, it is not a simple task to implement appropriate boundary conditions.

To overcome the drawbacks of LBM, which is applied globally in the whole flow domain, a lattice Boltzmann flux solver (LBFS) [32] was recently developed, which only applies LBM locally. In LBFS, the Finite Volume Method (FVM) is applied to solve the macroscopic N-S equations, while the lattice Boltzmann method is implemented locally at each cell interface to calculate the fluxes. Based on the Chapman-Enskog (C-E) expansion analysis, the macroscopic flux can be evaluated from the LBE solutions. One of important contributions in LBFS is to approximate the non-equilibrium distribution function by the difference of two equilibrium distribution functions at two different locations and time levels. This way is much simpler than the conventional treatments with various expansion terms. Within the LBFS, only macroscopic flow variables are stored, and the physical boundary conditions can be easily implemented. At the same time, by introducing the LBM solver on the interface, the approximation of the high-order nonlin-

ear terms in N-S equations is avoided; and the pressure can be conveniently evaluated explicitly from the equation of state, rather than implicitly from the complex pressure Poisson equation in conventional N-S solvers. With the above advantages, LBFS has been successfully applied in the simulations of incompressible isothermal and thermal flows [33,34], and multiphase flows [35].

However, it should be noted that LBFS involves two sets of solvers [36]. Therefore, it is not very convenient for the researchers in LBM community to use this novel solver. Such constraint gives us the motivation to develop the present simplified lattice Boltzmann method (SLBM). In this method, by using lattice properties and the relationships given in C-E analysis, the solutions to the macroscopic governing equations are obtained by locally reconstructing LBE solution on the grid point. Similar to LBFS, the non-equilibrium distribution function is evaluated by the difference of the equilibrium distribution functions on local and surrounding points at two different time levels. The present SLBM inherits the merits of LBFS. To be specific, in SLBM, the equilibrium distribution function is calculated from the macroscopic variables; and the non-equilibrium distribution function is evaluated from the equilibrium distribution functions, i.e., also from the macroscopic variables. Therefore, the evolution of the distribution function is no longer needed in SLBM, which significantly lowers the requirement of virtual memories and facilitates the implementation of physical boundary conditions.

The present paper is laid out as follows. In Section 2, the N-S equations, the lattice Boltzmann equation and the Chapman-Enskog expansion analysis are briefly introduced. Section 3 gives the detailed description of the present method, and the implementation of boundary conditions. Analysis of the cost of virtual memories is conducted in Section 4. In Section 5, the stability performance of the present method is evaluated by numerical tests. Several representative numerical examples, including the 2D Taylor-Green vortex flow, the Couette flow, the Poiseuille flow and the 2D lid-driven cavity flow, are posted in Section 6. And finally, some conclusions are drawn in Section 7.

2 Lattice Boltzmann equation to Navier-Stokes equation: Chapman-Enskog expansion analysis

2.1 Navier-Stokes equations

For general isothermal fluid problems, the macroscopic governing equations are the Navier-Stokes equations [37], expressed as:

$$\frac{\partial \rho}{\partial t} + \nabla \cdot \rho \mathbf{u} = 0, \quad (2.1a)$$

$$\frac{\partial \rho \mathbf{u}}{\partial t} + \nabla \cdot (\rho \mathbf{u} \mathbf{u}) = -\nabla p + \nu \nabla \cdot [\nabla \rho \mathbf{u} + (\nabla \rho \mathbf{u})^T], \quad (2.1b)$$

where ρ is the density; u is the velocity vector; p and ν denote the pressure and the kinematic viscosity, respectively. In the above equations, since the density is variable,

the fluid is actually considered to be compressible. Therefore, to simulate incompressible flows, the above equations need to fulfill certain incompressible limit, i.e., the density variation is small and the Mach number is low.

2.2 Lattice Boltzmann equation

The conventional lattice Boltzmann equation with BGK approximation, or simply called the LBGK model [29], can be expressed as

$$f_\alpha(\mathbf{r} + \mathbf{e}_\alpha \delta t, t + \delta t) = f_\alpha(\mathbf{r}, t) + \frac{f_\alpha^{eq}(\mathbf{r}, t) - f_\alpha(\mathbf{r}, t)}{\tau}, \quad \alpha = 0, 1, \dots, N, \quad (2.2)$$

where f_α is the density distribution function along the α direction and f_α^{eq} is its corresponding equilibrium state; δt is the streaming time step; τ is the single relaxation parameter in the BGK model; and N is the number of the streaming directions. The macroscopic physical properties are obtained from the conservation laws of the mass and the momentum, i.e.,

$$\rho = \sum_\alpha f_\alpha, \quad \rho \mathbf{u} = \sum_\alpha f_\alpha \mathbf{e}_\alpha. \quad (2.3)$$

And the equilibrium density distribution function is expressed as:

$$f_\alpha^{eq} = \rho \omega_\alpha \left[1 + \frac{\mathbf{e}_\alpha \cdot \mathbf{u}}{c_s^2} + \frac{(\mathbf{e}_\alpha \cdot \mathbf{u})^2 - (c_s |\mathbf{u}|)^2}{2c_s^4} \right]. \quad (2.4)$$

LBGK is associated with a specific lattice velocity model. For 2D problems, one popular lattice velocity model is D2Q9 model [2]. As shown in Fig. 1, the lattice vectors of D2Q9 model are given by

$$\mathbf{e}_\alpha = \begin{cases} 0, & \alpha = 0, \\ (\pm 1, 0), (0, \pm 1), & \alpha = 1, 2, 3, 4, \\ (\pm 1, \pm 1), & \alpha = 5, 6, 7, 8. \end{cases} \quad (2.5)$$

The weight ω_α and the sound speed c_s are

$$\omega_0 = \frac{4}{9}, \quad \omega_{1-4} = \frac{1}{9}, \quad \omega_{5-8} = \frac{1}{36}, \quad c_s = \frac{c}{\sqrt{3}}, \quad (2.6)$$

where $c = \delta x / \delta t$ is set to be 1 here, and δx is the lattice spacing.

2.3 Chapman-Enskog expansion analysis

Both the Navier-Stokes equations and the lattice Boltzmann equation are mathematical expressions for the same fluid problem. Therefore, there should exist certain links

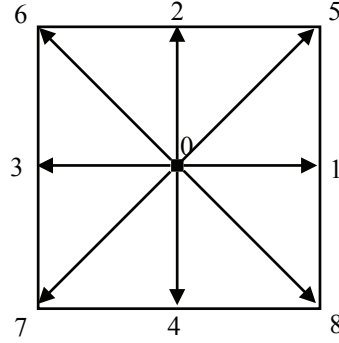


Figure 1: Illustrations of the D2Q9 model.

between these two systems. Chapman-Enskog (C-E) expansion analysis is such a link [38,39].

The basic idea in the Chapman-Enskog expansion analysis is the multi-scale expansion. Accordingly, the density distribution function, the temporal derivative and the spatial derivative can be expanded as:

$$f_\alpha = f_\alpha^{(0)} + \varepsilon f_\alpha^{(1)} + \varepsilon^2 f_\alpha^{(2)}, \quad (2.7a)$$

$$\frac{\partial}{\partial t} = \varepsilon \frac{\partial}{\partial t_0} + \varepsilon^2 \frac{\partial}{\partial t_1}, \quad (2.7b)$$

$$\nabla_r = \varepsilon \nabla_{r1}, \quad (2.7c)$$

where ε is a small parameter proportional to the Knudsen number [40]. By using the truncated Taylor series expansion, the lattice Boltzmann equation (2.2) can be reduced to the following formulation with the second-order of accuracy both in time and in space:

$$\left(\frac{\partial}{\partial t} + \mathbf{e}_\alpha \cdot \nabla \right) f_\alpha + \frac{\delta_t}{2} \left(\frac{\partial}{\partial t} + \mathbf{e}_\alpha \cdot \nabla \right)^2 f_\alpha + \frac{1}{\tau \delta_t} (f_\alpha - f_\alpha^{eq}) + \mathcal{O}(\delta_t^2) = 0. \quad (2.8)$$

Substituting the multi-scale expansions (Eqs. (2.7a), (2.7b) and (2.7c)) into the above equation, gives the following formulations at different orders of ε :

$$\mathcal{O}(\varepsilon^0): \quad (f_\alpha^{(0)} - f_\alpha^{eq}) / (\tau \delta_t) = 0, \quad (2.9a)$$

$$\mathcal{O}(\varepsilon^1): \quad \left(\frac{\partial}{\partial t_0} + \mathbf{e}_\alpha \cdot \nabla_1 \right) f_\alpha^{(0)} + \frac{1}{\tau \delta_t} f_\alpha^{(1)} = 0, \quad (2.9b)$$

$$\mathcal{O}(\varepsilon^2): \quad \frac{\partial f_\alpha^{(0)}}{\partial t_1} + \left(1 - \frac{1}{2\tau} \right) \left(\frac{\partial}{\partial t_0} + \mathbf{e}_\alpha \cdot \nabla_1 \right) f_\alpha^{(1)} + \frac{1}{\tau \delta_t} f_\alpha^{(2)} = 0. \quad (2.9c)$$

From Eq. (2.9a), it is obtained that

$$f_\alpha^{(0)} = f_\alpha^{eq}. \quad (2.10)$$

And Eq. (2.9b) gives

$$\varepsilon f_{\alpha}^{(1)} = -\tau \delta_t \varepsilon \left(\frac{\partial}{\partial t_0} + \mathbf{e}_{\alpha} \cdot \nabla_1 \right) f_{\alpha}^{eq}. \quad (2.11)$$

By summing up Eqs. (2.9b) and (2.9c) in all lattice velocity directions, and combining the obtained formulations in time scales t_0 and t_1 , the following equation is derived

$$\frac{\partial \rho}{\partial t} + \nabla \cdot \left(\sum_{\alpha} \mathbf{e}_{\alpha} f_{\alpha}^{eq} \right) = 0. \quad (2.12)$$

Similarly, by taking summation of the first-moment of Eqs. (2.9b) and (2.9c) in all lattice velocity directions, and combining the obtained formulations in time scales t_0 and t_1 , it can be derived that

$$\frac{\partial \rho \mathbf{u}}{\partial t} + \nabla \cdot \Pi = 0, \quad (2.13)$$

where Π is the momentum flux tensor, expressed as

$$\Pi_{\beta\gamma} = \sum_{\alpha} (\mathbf{e}_{\alpha})_{\beta} (\mathbf{e}_{\alpha})_{\gamma} \left[f_{\alpha}^{eq} + \left(1 - \frac{1}{2\tau} \right) \varepsilon f_{\alpha}^{(1)} \right], \quad (2.14)$$

$(\mathbf{e}_{\alpha})_{\beta}$ and $(\mathbf{e}_{\alpha})_{\gamma}$ are the components of the lattice velocity vector (\mathbf{e}_{α}) in the β -direction and the γ -direction, respectively. From Eq. (2.7a), it is shown that to the first order of ε , the distribution function f_{α} is approximated by $f_{\alpha}^{eq} + \varepsilon f_{\alpha}^{(1)}$. So we can rewrite Eqs. (2.11) and (2.14) into

$$f_{\alpha}^{neq} = f_{\alpha} - f_{\alpha}^{eq} = \varepsilon f_{\alpha}^{(1)} = -\tau \delta_t \left(\frac{\partial}{\partial t} + \mathbf{e}_{\alpha} \cdot \nabla \right) f_{\alpha}^{eq} = -\tau \delta_t D f_{\alpha}^{eq}, \quad (2.15a)$$

$$\Pi_{\beta\gamma} = \sum_{\alpha} (\mathbf{e}_{\alpha})_{\beta} (\mathbf{e}_{\alpha})_{\gamma} \left[f_{\alpha}^{eq} + \left(1 - \frac{1}{2\tau} \right) f_{\alpha}^{neq} \right], \quad (2.15b)$$

where f_{α}^{neq} is the non-equilibrium distribution function; and according to the conservation laws, it fulfills the following relationships:

$$\sum_{\alpha} f_{\alpha}^{neq} = 0, \quad \sum_{\alpha} \mathbf{e}_{\alpha} f_{\alpha}^{neq} = 0. \quad (2.16)$$

In this case, Eqs. (2.12) and (2.13) recover the macroscopic N-S equations (2.1a) and (2.1b) [41] with the following relationship between the single relaxation parameter τ and the kinematic viscosity ν

$$\nu = c_s^2 \left(\tau - \frac{1}{2} \right) \delta_t. \quad (2.17)$$

3 Simplified Lattice Boltzmann Method (SLBM) without evolution of distribution function

3.1 Formulations of SLBM

In the previous section, it is shown that for isothermal incompressible flows, the governing equations recovered by LBM are

$$\frac{\partial \rho}{\partial t} + \nabla \cdot \left(\sum_{\alpha} \mathbf{e}_{\alpha} f_{\alpha}^{eq} \right) = 0, \quad (3.1a)$$

$$\frac{\partial \rho \mathbf{u}}{\partial t} + \nabla \cdot \left[\sum_{\alpha} (\mathbf{e}_{\alpha})_{\beta} (\mathbf{e}_{\alpha})_{\gamma} f_{\alpha}^{eq} + \left(1 - \frac{1}{2\tau} \right) \sum_{\alpha} (\mathbf{e}_{\alpha})_{\beta} (\mathbf{e}_{\alpha})_{\gamma} f_{\alpha}^{neq} \right] = 0. \quad (3.1b)$$

With the help of the fractional step technique [42], the above equations can be solved by the following predictor-corrector scheme:

Predictor step:

$$\frac{\partial \rho}{\partial t} + \nabla \cdot \left(\sum_{\alpha} \mathbf{e}_{\alpha} f_{\alpha}^{eq} \right) = 0, \quad (3.2a)$$

$$\frac{\partial \rho \mathbf{u}}{\partial t} + \nabla \cdot \left[\sum_{\alpha} (\mathbf{e}_{\alpha})_{\beta} (\mathbf{e}_{\alpha})_{\gamma} f_{\alpha}^{eq} + \frac{1}{2\tau} \sum_{\alpha} (\mathbf{e}_{\alpha})_{\beta} (\mathbf{e}_{\alpha})_{\gamma} f_{\alpha}^{neq} \right] = 0. \quad (3.2b)$$

Corrector step:

$$\frac{\partial \rho}{\partial t} = 0, \quad (3.3a)$$

$$\frac{\partial \rho \mathbf{u}}{\partial t} + \nabla \cdot \left[\left(1 - \frac{1}{\tau} \right) \sum_{\alpha} (\mathbf{e}_{\alpha})_{\beta} (\mathbf{e}_{\alpha})_{\gamma} f_{\alpha}^{neq} \right] = 0. \quad (3.3b)$$

Now, we wish to reconstruct the LBE solutions to recover the above equations. In the predictor step, the intermediate density and velocity can be computed by the following formulations:

$$\rho^* = \sum_{\alpha} f_{\alpha}^{eq}(\mathbf{r} - \mathbf{e}_{\alpha} \delta_t, t - \delta_t), \quad (3.4a)$$

$$\rho^* \mathbf{u}^* = \sum_{\alpha} \mathbf{e}_{\alpha} f_{\alpha}^{eq}(\mathbf{r} - \mathbf{e}_{\alpha} \delta_t, t - \delta_t). \quad (3.4b)$$

It can be proven that the above equations are able to recover the macroscopic governing equations (3.2a)-(3.2b) in the predictor step with the second-order of accuracy in space and time. Applying Taylor series expansion to the distribution function with the third-order truncated error in space and time leads to:

$$\begin{aligned} f_{\alpha}^{eq}(\mathbf{r} - \mathbf{e}_{\alpha} \delta_t, t - \delta_t) &= f_{\alpha}^{eq}(\mathbf{r}, t) - \delta_t D f_{\alpha}^{eq}(\mathbf{r}, t) + \frac{\delta_t^2}{2} D^2 f_{\alpha}^{eq}(\mathbf{r}, t) + \mathcal{O}(\delta_t^3) \\ &= f_{\alpha}^{eq}(\mathbf{r}, t) - \delta_t D f_{\alpha}^{eq}(\mathbf{r}, t) - \frac{\delta_t}{2\tau} D f_{\alpha}^{neq}(\mathbf{r}, t) + \mathcal{O}(\delta_t^3). \end{aligned} \quad (3.5)$$

Note that Eq. (2.15a) has been applied in Eq. (3.5). Substituting Eq. (3.5) into Eq. (3.4a), yields:

$$\begin{aligned} \rho^* = & \sum_{\alpha} f_{\alpha}^{eq}(\mathbf{r}, t) - \delta_t \left[\frac{\partial}{\partial t} \sum_{\alpha} f_{\alpha}^{eq}(\mathbf{r}, t) + \nabla \cdot \left(\sum_{\alpha} \mathbf{e}_{\alpha} f_{\alpha}^{eq} \right) \right] \\ & - \frac{\delta_t}{2\tau} \left[\frac{\partial}{\partial t} \left(\sum_{\alpha} f_{\alpha}^{neq}(\mathbf{r}, t) \right) + \nabla \cdot \left(\sum_{\alpha} \mathbf{e}_{\alpha} f_{\alpha}^{neq}(\mathbf{r}, t) \right) \right] + \mathcal{O}(\delta_t^3). \end{aligned} \quad (3.6)$$

Note that from the conservation law, the first term on the Right-Hand-Side (RHS) is the density at (\mathbf{r}, t) , which can be considered as ρ^* . According to the features of the non-equilibrium distribution function (Eq. (2.16)), the third term on RHS vanishes. Overall, Eq. (3.6) can be simplified to

$$\frac{\partial \rho}{\partial t} + \nabla \cdot \left(\sum_{\alpha} \mathbf{e}_{\alpha} f_{\alpha}^{eq} \right) + \mathcal{O}(\delta_t^2) = 0. \quad (3.7)$$

The above equation shows that Eq. (3.4a) can recover Eq. (3.2a) with the second-order of accuracy in space and time.

Similarly, substituting Eq. (3.5) into Eq. (3.4b), gives

$$\begin{aligned} \rho^* \mathbf{u}^* = & \sum_{\alpha} \mathbf{e}_{\alpha} f_{\alpha}^{eq}(\mathbf{r}, t) - \delta_t \left[\frac{\partial}{\partial t} \sum_{\alpha} \mathbf{e}_{\alpha} f_{\alpha}^{eq}(\mathbf{r}, t) + \nabla \cdot \sum_{\alpha} (\mathbf{e}_{\alpha})_{\beta} (\mathbf{e}_{\alpha})_{\gamma} f_{\alpha}^{eq}(\mathbf{r}, t) \right] \\ & - \frac{\delta_t}{2\tau} \sum_{\alpha} \mathbf{e}_{\alpha} D f_{\alpha}^{neq}(\mathbf{r}, t) + \mathcal{O}(\delta_t^3). \end{aligned} \quad (3.8)$$

According to the conservation law, the first term on RHS can be considered as $\rho^* \mathbf{u}^*$. The third term on RHS can be simplified by the features of the non-equilibrium distribution function (Eq. (2.16)) into

$$\sum_{\alpha} \mathbf{e}_{\alpha} D f_{\alpha}^{neq}(\mathbf{r}, t) = \nabla \cdot \left[\sum_{\alpha} (\mathbf{e}_{\alpha})_{\beta} (\mathbf{e}_{\alpha})_{\gamma} f_{\alpha}^{neq}(\mathbf{r}, t) \right]. \quad (3.9)$$

Therefore, Eq. (3.8) can be reduced to

$$\frac{\partial \rho \mathbf{u}}{\partial t} + \nabla \cdot \left[\sum_{\alpha} (\mathbf{e}_{\alpha})_{\beta} (\mathbf{e}_{\alpha})_{\gamma} f_{\alpha}^{eq} + \frac{1}{2\tau} \sum_{\alpha} (\mathbf{e}_{\alpha})_{\beta} (\mathbf{e}_{\alpha})_{\gamma} f_{\alpha}^{neq} \right] + \mathcal{O}(\delta_t^2) = 0. \quad (3.10)$$

Eq. (3.10) shows that Eq. (3.4b) recovers Eq. (3.2b) with the second-order of accuracy in space and time.

In the corrector step, the final density and velocity are evaluated by

$$\rho(\mathbf{r}, t) = \rho^*, \quad (3.11a)$$

$$\rho(\mathbf{r}, t) \mathbf{u}(\mathbf{r}, t) = \rho^* \mathbf{u}^* + \left(1 - \frac{1}{\tau} \right) \sum_{\alpha} \mathbf{e}_{\alpha} f_{\alpha}^{neq}(\mathbf{r} - \mathbf{e}_{\alpha} \delta_t, t). \quad (3.11b)$$

Similar to the procedure in the predictor step, it can be proven that Eq. (3.11a) recovers Eq. (3.3a) exactly. Now, we look at the last term in Eq. (3.11b). Using Taylor series expansion, $f_\alpha^{neq}(\mathbf{r} - \mathbf{e}_\alpha \delta_t, t)$ can be approximated by

$$\begin{aligned} f_\alpha^{neq}(\mathbf{r} - \mathbf{e}_\alpha \delta_t, t) &= f_\alpha^{neq}(\mathbf{r}, t) - \delta_t \nabla f_\alpha^{neq}(\mathbf{r}, t) + \frac{\delta_t^2}{2} \nabla^2 f_\alpha^{neq}(\mathbf{r}, t) + \mathcal{O}(\delta_t^3) \\ &= f_\alpha^{neq}(\mathbf{r}, t) - \delta_t \nabla f_\alpha^{neq}(\mathbf{r}, t) - \frac{\delta_t^3}{2} \tau \nabla^2 [D f_\alpha^{eq}(\mathbf{r}, t)] + \mathcal{O}(\delta_t^3) \\ &= f_\alpha^{neq}(\mathbf{r}, t) - \delta_t \nabla f_\alpha^{neq}(\mathbf{r}, t) + \mathcal{O}(\delta_t^3). \end{aligned} \quad (3.12)$$

Note that Eq. (2.15a) has been used in the simplification of the above equation. As a consequence, the last term of Eq. (3.11b) can be written as

$$\begin{aligned} &\left(1 - \frac{1}{\tau}\right) \frac{1}{\delta_t} \sum_\alpha \mathbf{e}_\alpha f_\alpha^{neq}(\mathbf{r} - \mathbf{e}_\alpha \delta_t, t) \\ &= \left(1 - \frac{1}{\tau}\right) \frac{1}{\delta_t} \sum_\alpha \mathbf{e}_\alpha f_\alpha^{neq}(\mathbf{r}, t) - \left(1 - \frac{1}{\tau}\right) \left[\frac{\partial}{\partial t} \sum_\alpha \mathbf{e}_\alpha f_\alpha^{neq}(\mathbf{r}, t) \right. \\ &\quad \left. + \nabla \cdot \sum_\alpha (\mathbf{e}_\alpha)_\beta (\mathbf{e}_\alpha)_\gamma f_\alpha^{neq}(\mathbf{r}, t) \right] + \mathcal{O}(\delta_t^2). \end{aligned} \quad (3.13)$$

Using Eq. (2.16), Eq. (3.13) can be further reduced to

$$\left(1 - \frac{1}{\tau}\right) \frac{1}{\delta_t} \sum_\alpha \mathbf{e}_\alpha f_\alpha^{neq}(\mathbf{r} - \mathbf{e}_\alpha \delta_t, t) = -\nabla \cdot \left[\left(1 - \frac{1}{\tau}\right) \sum_\alpha (\mathbf{e}_\alpha)_\beta (\mathbf{e}_\alpha)_\gamma f_\alpha^{neq}(\mathbf{r}, t) \right] + \mathcal{O}(\delta_t^2). \quad (3.14)$$

Obviously, Eq. (3.14) recovers the last term of Eq. (3.3b) with the second-order of accuracy in space and time. Overall, it can be proven that Eq. (3.11b) can recover Eq. (3.3b) with the second-order of accuracy in space. For easy applications, the basic formulations of SLBM are summarized below:

Predictor step:

$$\rho^* = \sum_\alpha f_\alpha^{eq}(\mathbf{r} - \mathbf{e}_\alpha \delta_t, t - \delta_t), \quad (3.15a)$$

$$\rho^* \mathbf{u}^* = \sum_\alpha \mathbf{e}_\alpha f_\alpha^{eq}(\mathbf{r} - \mathbf{e}_\alpha \delta_t, t - \delta_t). \quad (3.15b)$$

Corrector step:

$$\rho(\mathbf{r}, t) = \rho^*, \quad (3.16a)$$

$$\rho(\mathbf{r}, t) \mathbf{u}(\mathbf{r}, t) = \rho^* \mathbf{u}^* + \left(1 - \frac{1}{\tau}\right) \sum_\alpha \mathbf{e}_\alpha f_\alpha^{neq}(\mathbf{r} - \mathbf{e}_\alpha \delta_t, t). \quad (3.16b)$$

In the application of above formulations, we need to calculate the non-equilibrium distributions. Inspired by LBFS, by recalling Eq. (2.15a) given in C-E analysis, the non-equilibrium density distribution function is approximated in a simple way by

$$f_\alpha^{neq}(\mathbf{r}, t) = -\tau \delta_t D f_\alpha^{eq}(\mathbf{r}, t) = -\tau [f_\alpha^{eq,*}(\mathbf{r}, t) - f_\alpha^{eq}(\mathbf{r} - \mathbf{e}_\alpha \delta_t, t - \delta_t)]. \quad (3.17)$$

Note that the equilibrium distribution function $f_{\alpha}^{eq,*}(r,t)$ used in the above equation is evaluated from the intermediate density and velocity obtained in the predictor step.

To sum up, in this section, we show the detailed derivation process of the simplified lattice Boltzmann method (SLBM). Based on the macroscopic governing equations recovered from the Chapman-Enskog expansion analysis and resolved by the fractional step method, the macroscopic solutions are reconstructed within LBM framework. The resultant formulations of SLBM only involve the equilibrium and non-equilibrium distribution functions. And in practical computations, the equilibrium distribution function is calculated from the macroscopic fluid properties, while the non-equilibrium distribution function is evaluated from the difference of two equilibrium distribution functions. Therefore, the time marching of SLBM is reflected in the evolution of the macroscopic fluid properties; and the evolution of the distribution function is no longer needed. Such characteristic gives SLBM various merits, e.g., easy implementation of the physical boundary conditions and lower requirement of virtual memory, which will be discussed in the following sections.

3.2 Implementation of boundary conditions

In the present method, the macroscopic physical properties on the boundaries are used in the calculation of the equilibrium distribution function. And in the corrector step, it is also necessary to know the non-equilibrium distribution functions on the boundaries. Therefore, appropriate boundary conditions for both the macroscopic properties and the non-equilibrium distribution function are required.

The boundary conditions of the macroscopic physical properties are similar to those applied in conventional N-S solvers [43]. The most common boundary conditions include the Dirichlet boundary condition and the Neumann boundary condition. For the Dirichlet boundary condition, a particular value for the fluid property is assigned on the boundary grid point. For the Neumann boundary condition, usually several inner layers of grid points are used to ensure the desired order of accuracy.

Now, we focus on the implementation of the boundary condition for the non-equilibrium distribution function, which is used in the corrector step. As pointed out by Chen et al. [9], the lattice Boltzmann method can be regarded as "a special finite difference" approximation of the Boltzmann equation which is related to the distribution function. Under this point of view, the distribution function, as well as its two components (the equilibrium part and the non-equilibrium part), are all considered to be continuous over the physical space. Therefore, the extrapolation scheme can be applied to estimate the boundary values of the non-equilibrium distribution functions.

The non-equilibrium extrapolation scheme was initially proposed by Guo et al. [5], and has been successfully applied in various problems. Specifically, in this boundary treatment, the non-equilibrium distribution function on the solid boundary is set equal to that on the inner layer of grid. According to Guo et al.'s analysis [5], the non-equilibrium

extrapolation scheme ensures the second-order of accuracy in space, i.e.,

$$f_{\alpha}^{neq}(\mathbf{x}_b) - f_{\alpha}^{neq}(\mathbf{x}_f) \sim \delta_x^2. \quad (3.18)$$

In this paper, we propose a linear extrapolation scheme for the non-equilibrium distribution function. Inspired by the comments of Chen et al. [9], the non-equilibrium distribution function is considered to be continuous over the whole computational domain. Therefore, the boundary values of the non-equilibrium distribution function can be obtained from linear extrapolation of the values on two inner layers of grids points, i.e.,

$$f_{\alpha}^{neq}(x_b) = f_{\alpha}^{neq}(x_{f1}) + [f_{\alpha}^{neq}(x_{f1}) - f_{\alpha}^{neq}(x_{f2})] \frac{x_{ib} - x_{ib-1}}{x_{ib-1} - x_{ib-2}}, \quad (3.19)$$

where x_b denotes the boundary point; x_{f1} and x_{f2} represent the locations of the first and the second inner layers of grid points, respectively. Specifically, on uniform meshes, the above formulation can be simplified as:

$$f_{\alpha}^{neq}(x_b) = 2f_{\alpha}^{neq}(x_{f1}) - f_{\alpha}^{neq}(x_{f2}). \quad (3.20)$$

To study the order of accuracy of this linear extrapolation scheme, we start from the Chapman-Enskog (C-E) expansion analysis. Based on C-E analysis, the non-equilibrium distribution function is in the order of $\mathcal{O}(\varepsilon)$, i.e.,

$$f_{\alpha}^{neq} = \tau \delta_t \left(\frac{\partial}{\partial t} + \mathbf{e}_{\alpha} \cdot \nabla \right) f_{\alpha}^{eq} \sim \delta_x f_{\alpha}^{(1)}, \quad (3.21)$$

where $f_{\alpha}^{(1)}$ comes from the multi-scale expansion of the distribution function and is at the same order of accuracy as f_{α}^{eq} . And through Taylor-series expansion, the functional values at the two inner layers of grid points can be expanded with respect to the boundary point as:

$$f_{\alpha}^{(1)}(x_{f1}) = f_{\alpha}^{(1)}(x_b) + \delta_x \frac{\partial f_{\alpha}^{(1)}(x_b)}{\partial x} + \mathcal{O}(\delta_x^2), \quad (3.22a)$$

$$f_{\alpha}^{(1)}(x_{f2}) = f_{\alpha}^{(1)}(x_b) + 2\delta_x \frac{\partial f_{\alpha}^{(1)}(x_b)}{\partial x} + \mathcal{O}(\delta_x^2). \quad (3.22b)$$

Substituting the above formulations into the linear extrapolation equation (3.20), yields

$$f_{\alpha}^{neq}(x_b) = \delta_x [2f_{\alpha}^{(1)}(x_{f1}) - f_{\alpha}^{(1)}(x_{f2})] = \delta_x f_{\alpha}^{(1)}(x_b) + \mathcal{O}(\delta_x^3). \quad (3.23)$$

Therefore, it is proven that the present scheme is able to achieve the third-order of accuracy in space. However, constrained by the second-order of accuracy in the main procedures of the simplified lattice Boltzmann method, the overall accuracy of our computation is still in the second order. Nevertheless, better computational results can be expected in cases with abrupt velocity changes near the solid boundaries by using Eq. (3.20), as presented in Section 6.2.

3.3 Computational sequence

The computational sequence of the present SLBM for the isothermal incompressible flow can be summarized as:

- Step 1 Specify the streaming distance δ_x ($\delta_x = \delta_t$). Determine the single relaxation parameter τ .
- Step 2 Predictor step. Use Eqs. (3.4a) and (3.4b) to calculate the intermediate physical properties ρ^* and \mathbf{u}^* .
- Step 3 Compute the non-equilibrium distribution function by applying Eq. (3.17).
- Step 4 Implement appropriate boundary conditions for the non-equilibrium distribution function.
- Step 5 Corrector step. Obtain the density and the velocity at the new time step from Eqs. (3.11a) and (3.11b).
- Step 6 Implement appropriate boundary conditions for the macroscopic physical properties.
- Step 7 Repeat Steps 2-6 until the computation converges or the prescribed maximum computational time is reached.

4 Memory cost

One important consideration in evaluating a new method is its memory cost. And it is also noted that one big drawback of the standard LBM is its high cost in virtual memories. In standard LBM, on one particular mesh point, the values of distribution functions along all lattice velocity directions need to be stored. For instance, with typical D2Q9 model, at least 9 variables on each mesh point shall be stored, which is a heavy burden when utilizing large amounts of mesh points. On the contrary, in the present simplified lattice Boltzmann method (SLBM), the macroscopic variables, instead of the distribution functions, are tracked during the computation, which implies that only the macroscopic variables need to be stored in virtual memories. In two-dimensional cases of incompressible isothermal flows, 6 variables are stored on each mesh point (present values and intermediate values of density and velocity). Therefore, theoretically SLBM can roughly save 33% of virtual memories.

However, it is also noteworthy that the practical amount of saved virtual memories depends on the tricks imposed in coding. For instance, it is decided by the code developer that whether the non-equilibrium distribution functions should be stored. Basically these tricks are the compromises between memory cost and computational efficiency. But in any way, comparing to the standard LBM, lower cost in virtual memories can be expected in the present SLBM.

5 Stability

Numerical stability is another standard to estimate the potential of a new numerical method. And the standard LBM is usually criticized for its poor numerical stability at high Reynolds number [44, 45]. In this section, the 2D lid-driven cavity flow at high Reynolds number is simulated to assess the stability performance of SLBM.

Consider a 2D cavity with the dimension of 1×1 . The upper lid is moving at a constant velocity of $U_{lid} = 0.1$. Physically, the fluid is driven by the moving lid to gradually form a circling flow inside the cavity. The flow can be considered at the steady state once the local velocity does not vary with time, which could be mathematically interpreted as the following convergence criteria

$$\frac{\sum_{ij} |(\sqrt{u^2 + v^2})^{n+1} - (\sqrt{u^2 + v^2})^n|}{\sum_{ij} (\sqrt{u^2 + v^2})^{n+1}} \leq \varepsilon, \quad (5.1)$$

where n denotes the number of the time level; u and v represent the horizontal and the vertical components of the velocity; ε is a small number, which is set to be 10^{-8} in this example.

In this problem, the Reynolds number, defined as

$$Re = U_{lid}L/v$$

is an important parameter to determine the flow pattern inside the cavity. Specifically, the Reynolds number is chosen as $Re = 7500$ in the present test. Under such high Reynolds number, the physical viscosity is very small. As a result, the single relaxation parameter τ is very close to the value of 0.5, posing great challenges to the numerical stability of the standard LBM [44, 45]. Usually, very fine meshes were applied to make the computation converge. In our numerical tests, to ensure the convergence of the standard LBM, 301×301 mesh resolution should be applied.

In the present stability test of SLBM, uniform meshes, with different resolutions of 301×301 , 201×201 , 101×101 and 11×11 , are applied. The snapshots of the streamlines and the velocity distributions along the centerlines are depicted in Figs. 2 and 3, respectively. The velocity profiles are compared with the data given by Ghia et al. [46]. It is shown that with mesh resolutions of 301×301 , SLBM is able to give both converged and accurate results. With mesh resolution higher than 101×101 , although losing some flow details (e.g., the second vortex on the right-bottom corner), the converged results are still reasonable in either flow patterns or velocity distributions. Even with mesh resolution as low as 11×11 , although the results are not accurate, converged results are well achieved by SLBM. Such performance indicates that SLBM is a very stable method, and therefore is more competitive than standard LBM in handling problems in high Reynolds number.

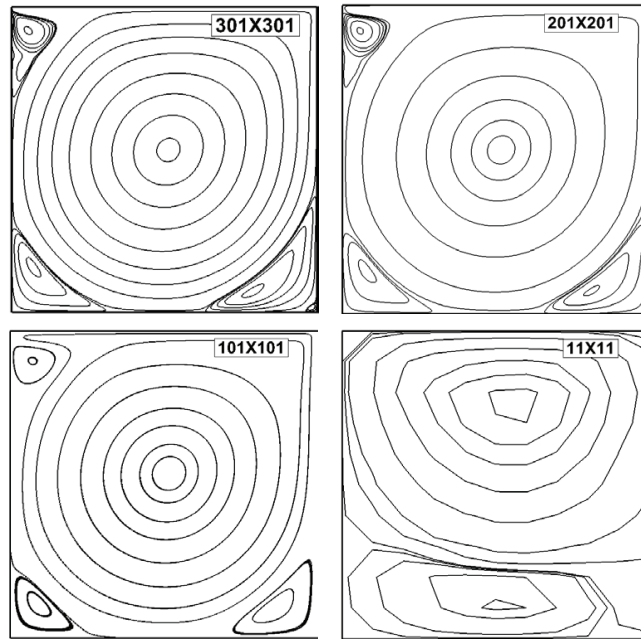


Figure 2: Snapshots of the final streamlines at $Re=7500$ using different mesh sizes.

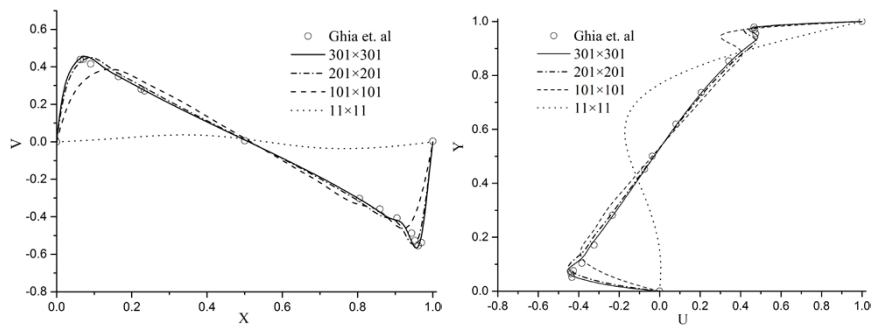


Figure 3: Velocity distributions along the centerlines at $Re=7500$.

6 Numerical examples

In this section, the simplified LBM (SLBM) is validated by several benchmark tests for the incompressible viscous flows. Firstly, the 2D Taylor-Green vortex flow is simulated under different mesh resolutions to study the order of accuracy. Then, the Couette flow with/without pressure gradient and the plane Poiseuille flow are simulated to further validate the robustness of the present method. Finally, the simplified lattice Boltzmann method is tested on the classical 2D lid-driven cavity flows at various Reynolds numbers. The simulation results are in good agreement with the analytical solutions or the

reference data in literatures, which proves the robustness of SLBM in simulating incompressible viscous flows.

6.1 2D Taylor-Green vortex flow

To examine the accuracy of the present simplified lattice Boltzmann method, firstly we study the two-dimensional Taylor-Green vortex flow [47]. In Taylor-Green vortex flow, the flow field consists of several periodic vortices decaying with time. The 2D Taylor-Green vortex flow has the following analytical solutions from the incompressible Navier-Stokes equations:

$$u(x,y,t) = -U_0 \cos(\pi x/L) \sin(\pi y/L) \exp\left(-\frac{2\pi^2 U_0 t}{ReL}\right), \quad (6.1a)$$

$$v(x,y,t) = U_0 \sin(\pi x/L) \cos(\pi y/L) \exp\left(-\frac{2\pi^2 U_0 t}{ReL}\right), \quad (6.1b)$$

$$p(x,y,t) = p_0 - \frac{\rho_0 U_0^2}{4} [\cos(2\pi x/L) + \sin(2\pi y/L)] \exp\left(-\frac{4\pi^2 U_0 t}{ReL}\right), \quad (6.1c)$$

where U_0 is the initial velocity amplitude; ν is the kinematic viscosity; $\rho_0 = 1.0$ is the reference density of the fluid; and p_0 is an arbitrary background pressure, which is set to be $p_0 = \rho_0 c_s^2$ in the present work.

The computational domain in our simulation is $[-L, L] \times [-L, L]$; and six different mesh sizes ($20 \times 20, 50 \times 50, 80 \times 80, 100 \times 100, 125 \times 125$ and 150×150) are taken for numerical simulation. Periodic boundary condition is applied on the four boundaries of the domain. The Reynolds number, defined as $Re = U_0 L / \nu$, is set to be 10. Solutions at the non-dimensional time $t^* = t(U_0/L) = 1.0$ are compared with the analytical solutions to study the relative error quantified by L_2 norm and defined as:

$$L_2 = \sqrt{\frac{\sum_{k=1}^{N \times N} \left(\frac{u_{\text{numerical}} - u_{\text{exact}}}{U_0} \right)^2}{N \times N}}, \quad (6.2)$$

where $u_{\text{numerical}}$ and u_{exact} refer to the numerical result and the analytical solution, respectively. The relationship between the L_2 norm and the mesh spacing h is presented in Fig. 4 in the log scale. The linear fitting of the scattered data gives the slope of 1.905, which indicates that the spatial accuracy of the present method is roughly in the second-order.

6.2 Benchmark tests of the flow between two parallel plates

The flow between two parallel plates is a classical problem in fluid mechanics [48, 49]. If the upper plate is moving with a constant velocity and the lower plate is stationary, the flow is called Couette flow; If both plates are stationary, and the fluid is driven by

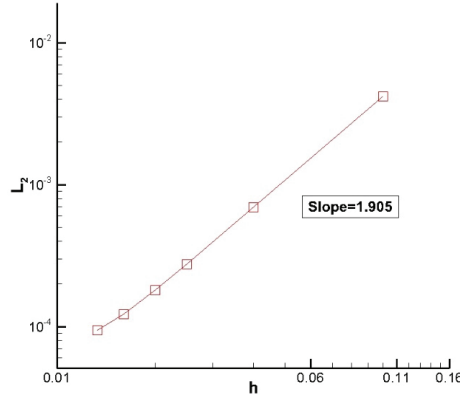


Figure 4: L_2 norm of relative error of u versus h for the decaying vortex flow.

a given pressure gradient, then the flow is named plane Poiseuille flow. For both kinds of problems, analytical solutions to the simplified N-S equations are available. Here, three benchmark tests, including the Couette flow with no pressure gradient, the Couette flow with the pressure gradient and the plane Poiseuille flow, are considered. The flow parameters adopted in our simulations are: plate distance $h=1$; the velocity of the upper plate $u_0=0.1$; the pressure gradient $\partial p/\partial x=-0.0001$; the dynamic viscosity $\mu=0.001$. For the Couette flow without the pressure gradient, the analytical solution is

$$u(y) = u_0 \frac{y}{h}. \quad (6.3)$$

And for the Couette flow with the pressure gradient, the analytical result is given by

$$u(y) = u_0 \frac{y}{h} + \frac{1}{2\mu} \left(\frac{\partial p}{\partial x} \right) (y^2 - hy). \quad (6.4)$$

Note that if u_0 is set to zero, then the above formula reduces to the solution for the plane Poiseuille flow.

The simplified lattice Boltzmann method proposed in this paper is applied to solve these problems. The mesh size applied here is 21×51 , with a uniform mesh spacing of $\Delta x = 0.02$. No-slip boundary condition is applied on the upper and the bottom walls, while periodic boundary condition is implemented on the left and the right boundaries. Fig. 5 shows the converged velocity profile in plane Poiseuille flow with different boundary treatments of the non-equilibrium distribution functions. Specifically, here we comparatively study the performance of the non-equilibrium extrapolation scheme developed by Guo et al. [5] and the linear extrapolation scheme proposed in this paper. As can be seen, through the linear extrapolation of the non-equilibrium distribution function, better agreement with the analytical results can be obtained. Fig. 6 presents the velocity profiles at the steady state of the Couette flows with or without the pressure gradient. It

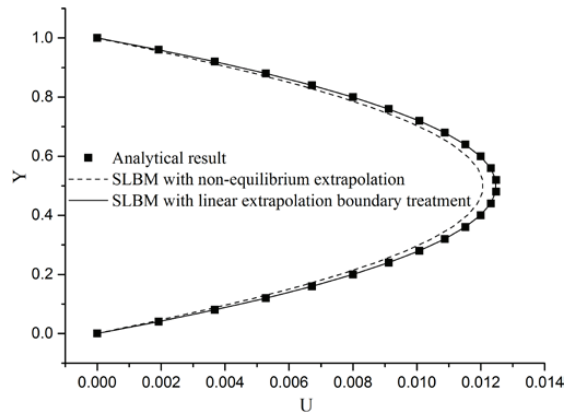


Figure 5: Comparisons of the velocity profiles of plane Poiseuille flow.

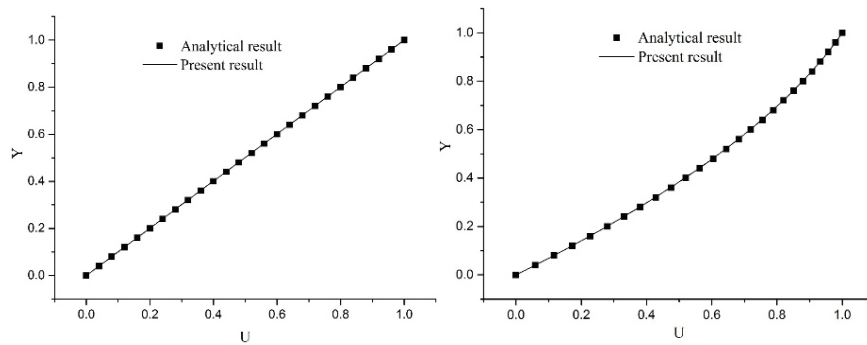


Figure 6: Comparisons of the velocity profiles at the steady state. Left: Couette flow with no pressure gradient; Right: Couette flow with pressure gradient.

is observed that in both cases, the computational results are in good accordance with the analytical values, which shows the good accuracy of the present method.

6.3 2D lid-driven cavity flow

In this section, the simplified lattice Boltzmann method is applied to simulate the 2D lid-driven cavity flow. The problem configuration, the definition of Reynolds number and the convergence criterion are the same as those discussed in Section 5. Here, three cases with Reynolds numbers of 1000, 5000 and 10000 are considered, which are solved using the uniform mesh sizes of 151×151 , 251×251 and 301×301 , respectively.

Table 1 gives the comparative results for the locations of primary vortex centers at different Reynolds numbers. It is observed that the vortex centers obtained by SLBM are in good agreement with the data in reference [46]. Quantitatively, the relative error between the present result and the reference data is within 1%, which indicates the good

Table 1: Comparisons for the locations of primary vortex centers at different Reynolds numbers.

| Re | Ghia et al. [46] | Present |
|-------|------------------|------------------|
| 1000 | (0.5313, 0.5625) | (0.5317, 0.5658) |
| 5000 | (0.5117, 0.5352) | (0.5155, 0.5347) |
| 10000 | (0.5117, 0.5333) | (0.5127, 0.5291) |

performance of the present method in predicting the flow field. Another common validation for lid-driven cavity flows is the comparison of the velocity distribution along the centerlines, as presented in Fig. 7. As can be seen, good agreements with the reference data are obtained both in the vertical velocity distribution along the y -centerline and in the horizontal velocity distribution along the x -centerline. The above tests give convincing evidences for the robustness of the present simplified LBM without evolution of the distribution function in simulating 2D incompressible viscous flows.

7 Concluding remarks

This paper presents a simplified lattice Boltzmann method (SLBM) without evolution of the distribution function for simulating isothermal incompressible viscous flows. The macroscopic governing equations recovered from lattice Boltzmann equation by using Chapman-Enskog (C-E) expansion analysis can be resolved by the predictor-corrector scheme. By using lattice properties and the relationships given by C-E analysis, SLBM reconstructs the solutions to these macroscopic equations with the second-order of accuracy in space. SLBM offers an alternative approach within the LBM framework and helps to eliminate many drawbacks of standard LBM. In practical computations, the equilibrium distribution function is computed from the macroscopic properties; and the non-equilibrium distribution function is evaluated from the difference of two equilibrium distribution functions at two different locations and time levels. Therefore, the macroscopic fluid properties, rather than the distribution function, are tracked during the computational process. Such treatments give several nice features to the present method: (1) there is no need to store the distribution function, which saves a lot of virtual memories; (2) the physical boundary conditions can be directly implemented.

The stability and the accuracy of the present method are studied numerically. For the numerical stability, numerical tests on 2D lid-driven cavity flow at high Reynolds number are conducted and it turns out that converged results can be acquired by SLBM even on very coarse meshes, which indicates the nice numerical stability of SLBM. The numerical accuracy of the SLBM is then studied through the classic Taylor-Green vortex flow. In this test, it is shown that the present method has approximately the second-order of accuracy in space.

More numerical tests, including Couette flow, Poiseuille flow and lid-driven cavity flow, are given as validation examples. Good agreements with the analytical value or reference data are observed in the results obtained by the present simplified lattice Boltz-

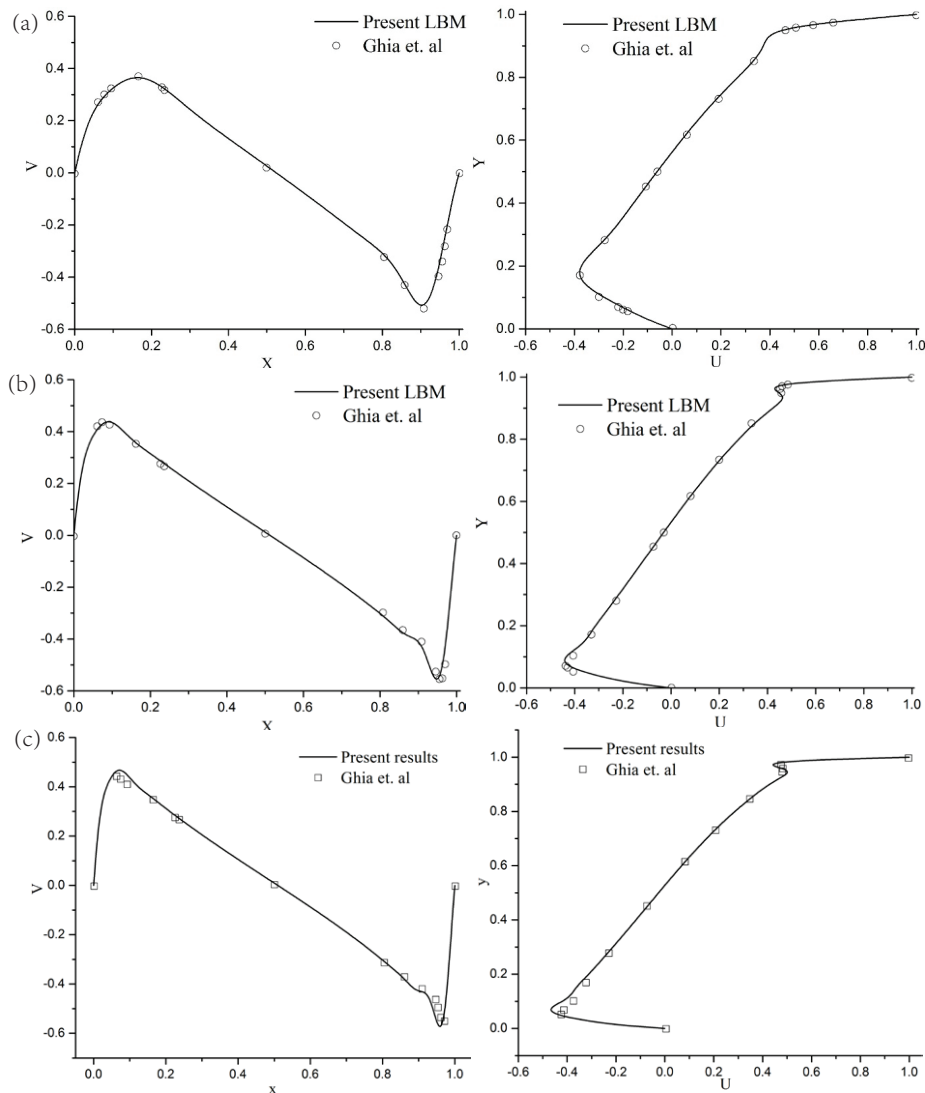


Figure 7: Comparisons of the velocity distribution. Left: x - V curve; Right: U - y curve. (a) $Re=1000$ (151×151); (b) $Re=5000$ (251×251); (c) $Re=10000$ (301×301).

mann method. These examples indicate that the SLBM presented in this paper is robust for isothermal incompressible viscous flows with comparatively lower memory cost and better numerical stability.

References

[1] S. CHEN, H. CHEN, D. MARTNEZ AND W. MATTHAEUS, *Lattice Boltzmann model for simula-*

- tion of magnetohydrodynamics*, Phys. Rev. Lett., 67 (1991), 3776.
- [2] Y. QIAN, D. D'HUMIÈRES AND P. LALLEMAND, *Lattice BGK models for Navier-Stokes equation*, EPL (Europhysics Letters), 17 (1992), 479.
 - [3] D. D'HUMIÈRES, *Multiplerelaxationtime lattice Boltzmann models in three dimensions*, Philosophical Transactions of the Royal Society of London A: Mathematical, Physical and Engineering Sciences, 360 (2002), pp. 437–451.
 - [4] R. MEI, L.-S. LUO AND W. SHYY, *An accurate curved boundary treatment in the lattice Boltzmann method*, J. Comput. Phys., 155 (1999), pp. 307–330.
 - [5] Z. GUO, C. ZHENG AND B. SHI, *An extrapolation method for boundary conditions in lattice Boltzmann method*, Phys. Fluids, 14 (2002), pp. 2007–2010.
 - [6] P. LALLEMAND AND L.-S. LUO, *Theory of the lattice Boltzmann method: Dispersion, dissipation, isotropy, Galilean invariance, and stability*, Phys. Rev. E, 61 (2000), 6546.
 - [7] X. HE AND G. DOOLEN, *Lattice Boltzmann method on curvilinear coordinates system: flow around a circular cylinder*, J. Comput. Phys., 134 (1997), pp. 306–315.
 - [8] H. CHEN, S. CHEN AND W. H. MATTHAEUS, *Recovery of the Navier-Stokes equations using a lattice-gas Boltzmann method*, Phys. Rev. A, 45 (1992), R5339.
 - [9] S. CHEN, D. MARTINEZ AND R. MEI, *On boundary conditions in lattice Boltzmann methods*, Phys. Fluids, 8 (1996), pp. 2527–2536.
 - [10] Z. GUO, B. SHI AND N. WANG, *Lattice BGK model for incompressible NavierStokes equation*, J. Comput. Phys., 165 (2000), pp. 288–306.
 - [11] C. SHU, X. NIU AND Y. CHEW, *Taylor series expansion and least squares-based lattice Boltzmann method: three-dimensional formulation and its applications*, Int. J. Modern Phys. C, 14 (2003), pp. 925–944.
 - [12] Z.-G. FENG AND E. E. MICHAELIDES, *The immersed boundary-lattice Boltzmann method for solving fluidparticles interaction problems*, J. Comput. Phys., 195 (2004), pp. 602–628.
 - [13] Y.-H. ZHANG, X.-J. GU, R. W. BARBER AND D. R. EMERSON, *Capturing Knudsen layer phenomena using a lattice Boltzmann model*, Phys. Rev. E, 74 (2006), 046704.
 - [14] X. SHAN, X.-F. YUAN AND H. CHEN, *Kinetic theory representation of hydrodynamics: a way beyond the NavierStokes equation*, J. Fluid Mech., 550 (2006), pp. 413–441.
 - [15] C. LIM, C. SHU, X. NIU AND Y. CHEW, *Application of lattice Boltzmann method to simulate microchannel flows*, Phys. Fluids, 14 (2002), pp. 2299–2308.
 - [16] X. HE, S. CHEN AND G. D. DOOLEN, *A novel thermal model for the lattice Boltzmann method in incompressible limit*, J. Comput. Phys., 146 (1998), pp. 282–300.
 - [17] Y. PENG, C. SHU AND Y. CHEW, *Simplified thermal lattice Boltzmann model for incompressible thermal flows*, Phys. Rev. E, 68 (2003), 026701.
 - [18] G. TANG, W. TAO AND Y. HE, *Lattice Boltzmann method for gaseous microflows using kinetic theory boundary conditions*, Phys. Fluids, 17 (2005), 058101.
 - [19] X. HE, S. CHEN AND R. ZHANG, *A lattice Boltzmann scheme for incompressible multiphase flow and its application in simulation of RayleighTaylor instability*, J. Comput. Phys., 152 (1999), pp. 642–663.
 - [20] X. SHAN AND H. CHEN, *Lattice Boltzmann model for simulating flows with multiple phases and components*, Phys. Rev. E, 47 (1993), 1815.
 - [21] T. INAMURO, T. OGATA, S. TAJIMA AND N. KONISHI, *A lattice Boltzmann method for incompressible two-phase flows with large density differences*, J. Comput. Phys., 198 (2004), pp. 628–644.
 - [22] X. SHAN, *Simulation of Rayleigh-Bénard convection using a lattice Boltzmann method*, Phys. Rev. E, 55 (1997), 2780.
 - [23] H. K. VERSTEEG AND W. MALALASEKERA, *An Introduction to Computational Fluid Dy-*

- namics: the Finite Volume Method, Pearson Education, 2007.
- [24] T. LISZKA AND J. ORKISZ, *The finite difference method at arbitrary irregular grids and its application in applied mechanics*, Comput. Struct., 11 (1980), pp. 83–95.
 - [25] C. B. LEE, *New features of CS solitons and the formation of vortices*, Phys. Lett. A, 247 (1998), pp. 397–402.
 - [26] C. LEE, *Possible universal transitional scenario in a flat plate boundary layer: Measurement and visualization*, Phys. Rev. E, 62 (2000), 3659.
 - [27] C. LEE AND R. LI, *Dominant structure for turbulent production in a transitional boundary layer*, J. Turbulence, (2007), N55.
 - [28] C. K. AIDUN AND J. R. CLAUSEN, *Lattice-Boltzmann method for complex flows*, Ann. Rev. Fluid Mech., 42 (2010), pp. 439–472.
 - [29] S. CHEN AND G. D. DOOLEN, *Lattice Boltzmann method for fluid flows*, Ann. Rev. Fluid Mech., 30 (1998), pp. 329–364.
 - [30] X. HE AND L.-S. LUO, *Theory of the lattice Boltzmann method: From the Boltzmann equation to the lattice Boltzmann equation*, Phys. Rev. E, 56 (1997), 6811.
 - [31] G. R. MCNAMARA AND G. ZANETTI, *Use of the Boltzmann equation to simulate lattice-gas automata*, Phys. Rev. Lett., 61 (1988), 2332.
 - [32] C. SHU, Y. WANG, C. TEO AND J. WU, *Development of lattice Boltzmann flux solver for simulation of incompressible flows*, Adv. Appl. Math. Mech., 6 (2014), pp. 436–460.
 - [33] Y. WANG, C. SHU AND C. TEO, *Development of LBGK and incompressible LBGK-based lattice Boltzmann flux solvers for simulation of incompressible flows*, Int. J. Numer. Methods Fluids, 75 (2014), pp. 344–364.
 - [34] Y. WANG, C. SHU AND C. TEO, *Thermal lattice Boltzmann flux solver and its application for simulation of incompressible thermal flows*, Comput. Fluids, 94 (2014) pp. 98–111.
 - [35] Y. WANG, C. SHU, H. HUANG AND C. TEO, *Multiphase lattice Boltzmann flux solver for incompressible multiphase flows with large density ratio*, J. Comput. Phys., 280 (2015), pp. 404–423.
 - [36] Y. WANG, L. YANG AND C. SHU, *From lattice Boltzmann method to lattice Boltzmann flux solver*, Entropy, 17 (2015), pp. 7713–7735.
 - [37] F. M. WHITE, Fluid Mechanics, McGraw-Hill, New York, 2003.
 - [38] R. BENZI, S. SUCCI AND M. VERGASSOLA, *The lattice Boltzmann equation: theory and applications*, Phys. Reports, 222 (1992), pp. 145–197.
 - [39] U. FRISCH, D. D’HUMIÈRES, B. HASSLACHER, P. LALLEMAND, Y. POMEAU AND J.-P. RIVET, *Lattice gas hydrodynamics in two and three dimensions*, Complex Systems, 1 (1987), pp. 649–707.
 - [40] T. INAMURO, M. YOSHINO AND F. OGINO, *Accuracy of the lattice Boltzmann method for small Knudsen number with finite Reynolds number*, Phys. Fluids, 9 (1997), pp. 3535–3542.
 - [41] Z. GUO AND C. SHU, Lattice Boltzmann Method and Its Applications in Engineering, World Scientific, 2013.
 - [42] J. KIM AND P. MOIN, *Application of a fractional-step method to incompressible Navier-Stokes equations*, J. Comput. Phys., 59 (1985), pp. 308–323.
 - [43] J. D. ANDERSON AND J. WENDT, Computational Fluid Dynamics, Springer, 1995.
 - [44] J. D. STERLING, S. CHEN, *Stability analysis of lattice Boltzmann methods*, J. Comput. Phys., 123 (1996), pp. 196–206.
 - [45] X. NIU, C. SHU, Y. CHEW AND T. WANG, *Investigation of stability and hydrodynamics of different lattice Boltzmann models*, J. Stat. Phys., 117 (2004), pp. 665–680.
 - [46] U. GHIA, K. N. GHIA AND C. SHIN, *High-Re solutions for incompressible flow using the Navier-*

- Stokes equations and a multigrid method*, J. Comput. Phys., 48 (1982), 387–411.
- [47] R. MEI, L.-S. LUO, P. LALLEMAND AND D. D’HUMIÈRES, *Consistent initial conditions for lattice Boltzmann simulations*, Comput. Fluids, 35 (2006), pp. 855–862.
- [48] R. MEI AND W. SHYY, *On the finite difference-based lattice Boltzmann method in curvilinear coordinates*, J. Comput. Phys., 143 (1998), pp. 426–448.
- [49] Z. GUO, C. ZHENG AND B. SHI, *Discrete lattice effects on the forcing term in the lattice Boltzmann method*, Phys. Rev. E, 65 (2002), 046308.